ELSEVIER

Cement & Concrete Composites 26 (2004) 765–775

Cement & Concrete Composites

www.elsevier.com/locate/cemconcomp

Flexural strengthening of RC continuous beams using CFRP laminates

A.F. Ashour *, S.A. El-Refaie, S.W. Garrity

Department of Civil and Environmental Engineering, University of Bradford, West Yorkshire BD7 1DP, UK

Received 24 July 2002; accepted 14 July 2003

Abstract

This paper presents test results at failure of 16 reinforced concrete (RC) continuous beams with different arrangements of internal steel bars and external carbon fibre reinforced polymer (CFRP) laminates. All test specimens had the same geometrical dimensions and were classified into three groups according to the amount of internal steel reinforcement. Each group included one unstrengthened control beam designed to fail in flexure. Different parameters including the length, thickness, position and form of the CFRP laminates were investigated. Three failure modes of beams with external CFRP laminates were observed, namely laminate rupture, laminate separation and peeling failure of the concrete cover attached to the laminate. The ductility of all strengthened beams was reduced compared with that of the respective unstrengthened control beam.

Simplified methods for estimating the flexural load capacity and the interface shear stresses between the adhesive and concrete at failure of beams tested are presented. Comparisons between results from experiments and those obtained from the simplified methods show that most beams were close to achieving their full flexural capacity and the longitudinal elastic shear stresses at the adhesive/concrete interface calculated at beam failure conformed to the limiting value recommended in the Concrete Society Technical Report 55.

1. Introduction

Using carbon fibre reinforced polymer (CFRP) laminates has proved to be an effective means of upgrading and strengthening reinforced concrete (RC) beams. However, premature failures such as peeling failure and laminate separation can significantly limit the capacity enhancement and prevent the full ultimate flexural capacity of the retrofitted beams from being attained. Laminate peeling or separation may occur due to the high longitudinal shear and transverse normal stresses at the plate end resulting from the abrupt curtailment of the plate [1,2].

Several studies were conducted to identify ways of preventing peeling failure with a view to improving the load capacity and ductility of strengthened concrete beams [2–6]. Garden and Hollaway [3] extended the plate ends under the end supports in order to obtain full plate end anchorage. It was found that plate separation was prevented but peeling failure of the concrete cover still occurred. Other researchers [2,4–6] studied the use of end anchorage techniques such as U-shape and L-shape jackets and steel bolts. Those end anchorage techniques increased the ultimate failure load, but did not prevent peeling failure.

Although many in situ RC beams are of continuous construction, there has been very little research into the behaviour of such beams with external reinforcement [4,7–9]. In addition, most design guidelines [10,11] were developed for simply supported beams with external fibre reinforced polymer laminates. The principal aims of this paper may be summarised as follows:

- to present test results at failure of 16 RC continuous beams strengthened with different arrangements of external CFRP laminates, including the analysis and discussion of different modes of failure, beam ductility and enhancement of load and moment capacities;
- to develop a simplified technique for estimating the flexural capacity of RC continuous beams strengthened with external CFRP laminates;

* Corresponding author. Tel.: +44-1274-233-870; fax: +44-1274-234-111.

E-mail address: afashour@bradford.ac.uk (A.F. Ashour).

0958-9465/$ - see front matter © 2003 Published by Elsevier Ltd.
doi:10.1016/j.cemconcomp.2003.07.002

Nomenclature

A_{fl}	area of CFRP at concrete crushing and tensile rupture of CFRP laminates
A_f	area of CFRP laminates
A_s	internal longitudinal tension steel reinforcement area
A'_s	internal longitudinal compression steel reinforcement area
b	section width
C	concrete compressive force
C_s	compressive force in steel reinforcement above the neutral axis
d	effective depth of internal longitudinal tension steel bars
d'	depth of internal longitudinal compression steel bars from the top face of the section
d_f	depth of CFRP laminates
E_s	Young's modulus of steel bars
E_f	elastic modulus of CFRP laminates
E_c	elastic modulus of concrete
f_{cu}	concrete compressive strength
f_f	tensile stresses of CFRP laminate
f_{fu}	ultimate strength of CFRP laminates
f_s	stress in tensile steel bars
f'_s	stress in compressive steel bars
f_y	yield strength of steel bars
f_u	ultimate strength of steel bars
k_1	ratio of the average compressive stress to the concrete cube strength f_{cu}
k_2	ratio of the depth of the idealised rectangular stress block to the neutral axis depth
L	beam span
L_1	length of the CFRP sheets over the central support
L_2	length of the CFRP sheets at the beam soffit
M_h	experimental negative flexural failure moment of test specimens
M_s	experimental positive flexural failure moment of test specimens
M_u	theoretical flexural strength of RC section with CFRP laminates
M_{us}	theoretical flexural capacity of mid-span section
M_{uh}	theoretical flexural capacity of central support section
M_{he}	theoretical negative flexural capacity of the unstrengthened section at the CFRP sheet end
M_{se}	theoretical positive flexural capacity of the unstrengthened section at the CFRP sheet end
n_f	external plate modular ratio
P_t	theoretical ultimate mid-span point load obtained from flexural mechanism
P_{th}	$2P_t$, total theoretical ultimate load on both spans obtained from flexural mechanism
P_u	experimental failure load of test specimens
Q	summation of the internal forces
T_s	tensile force in steel reinforcement below the neutral axis
T_f	tensile force in external CFRP laminates
t_f	thickness of CFRP laminates
V	shear force calculated at beam failure
x	neutral axis depth
y_f	depth of the CFRP plate measured from the neutral axis to the centroid of the plate
I_c	transformed second moment of area of the cracked plated reinforced concrete cross-section in terms of concrete
ξ	ultimate load enhancement ratio
η	ultimate moment enhancement ratio
τ	longitudinal shear stress at the adhesive level
μ_Δ	deflection ductility index
Δ_u	mid-span deflection at beam ultimate load
Δ_y	mid-span deflection at the lower yielding load of the tensile reinforcement over the central support or the beam mid-span
ε_c	concrete strain at the extreme compression fibre
ε_f	CFRP laminates strain at the extreme tension fibre
ε_{cu}	concrete crushing strain
ε_{fu}	tensile rupture strain
ε_s	tensile steel bar strain
ε'_s	compressive steel bar strain
λ_1	ratio between experimental failure load and flexural capacity of test specimens

- to calculate the reserve capacity of beams tested if premature failure was prevented;
- to compare the longitudinal elastic shear stresses along the adhesive/concrete interface at the beam failure with the limiting values suggested by the Concrete Society Technical Report 55 [11].

2. Test programme

The test specimens consisted of 16 RC continuous beams classified into three groups (H, S and E) according to the arrangement of the internal steel reinforcement as given in Table 1. Beams in group H

Table 1
Details of the test specimens

Group no.	Beam no.	Main longitudinal steel		Form of CFRP laminates	Top CFRP over the central support		Bottom CFRP at mid-span		f_{cu} (N/mm^2)
		Top	Bottom		No.	L_1 (m)	No.	L_2 (m)	
H	H1	2T8	2T20	–	–	–	–	–	24.0
	H2	2T8	2T20	CFRP sheets	2	2.0	–	–	43.5
	H3	2T8	2T20	CFRP sheets	6	2.0	–	–	33.0
	H4	2T8	2T20	CFRP sheets	10	2.0	–	–	33.2
	H5	2T8	2T20	CFRP sheets	6	1.0	–	–	46.0
	H6	2T8	2T20	CFRP sheets	2	3.0	2	1.0	44.0
S	S1	2T20	2T8	–	–	–	–	–	26.0
	S2	2T20	2T8	CFRP sheets	–	–	2	2.0	42.9
	S3	2T20	2T8	CFRP sheets	–	–	6	2.0	33.3
	S4	2T20	2T8	CFRP sheets	–	–	6	3.5	42.8
	S5	2T20	2T8	CFRP sheets	–	–	10	3.5	24.4
E	E1	2T16	2T16	–	–	–	–	–	24.0
	E2	2T16	2T16	CFRP plate	1	2.5	–	–	43.6
	E3	2T16	2T16	CFRP plate	–	–	1	3.5	47.8
	E4	2T16	2T16	CFRP plate	1	2.5	1	3.5	46.1
	E5	2T16	2T16	CFRP sheets	6	2.5	–	–	44.7

(H1–H6) were reinforced with two bars of 8 mm diameter on the top side of the beam and two bars of 20 mm diameter on the bottom side, whereas beams in group S (S1–S5) were reinforced with an opposite arrangement of the internal longitudinal steel reinforcement as given Table 1. The top steel reinforcement of beams in group E (E1–E5) was the same as the bottom steel reinforcement, each consisting of two 16 mm diameter bars. Vertical links of 6 mm bar diameter at 100 mm centres were provided throughout each beam length in order to prevent shear failure. All beams had the same geometrical dimensions: 150 mm wide × 250 mm deep × 8500 mm long. Beam geometry and reinforcement as well as the loading and support arrangement are illustrated in Fig. 1.

The position, length, thickness and form (sheets or plates) of the CFRP laminates were the main parameters investigated as summarised in Table 1. Beams H1, S1 and E1 had no external reinforcement and were used as control specimens. Beams E2, E3 and E4 were strengthened with CFRP plates of 1.2 mm thickness and 100 mm width; whereas the rest of the beams were strengthened with CFRP sheets, each layer of 0.117 mm thickness and 110 mm width. The top of the central region of beam E5 was strengthened with CFRP sheets (six layers of 0.702 mm total thickness × 110 mm wide × 2500 mm long) of the same tensile strength and length as that of the CFRP plate used for beam E2. The CFRP laminates applied to the top face of the beams were placed symmetrically about the central support and

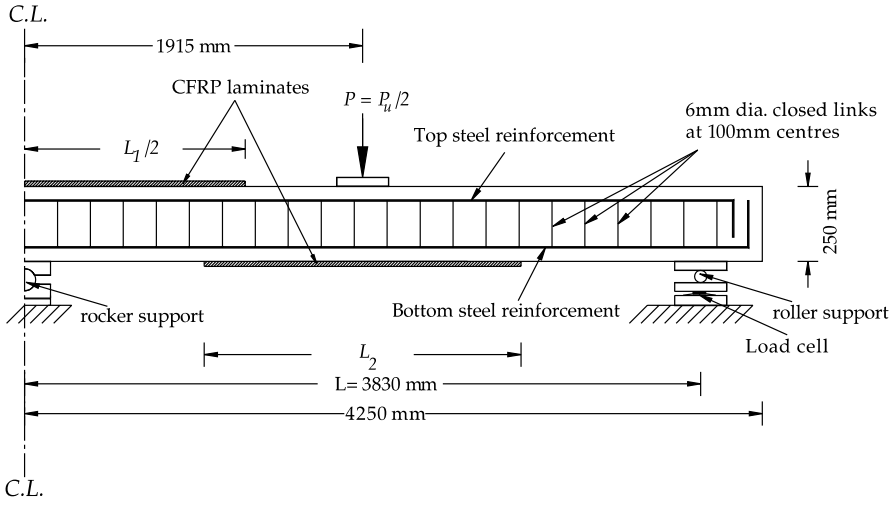

Fig. 1. Test set-up and strengthened RC beam details.

those applied to the bottom face of the beam were positioned symmetrically about the centres of both spans.

3. Material properties

The compressive strength f_{cu} of the concrete obtained for each beam from compression tests carried out on three 100 mm cubes is given in Table 1. The mechanical properties of the steel reinforcing bars used in the test beams were obtained by carrying out uniaxial tensile tests on three steel bar specimens. Table 2 shows the yield strength f_y, ultimate strength f_u and Young's modulus E_s obtained for different types of steel bars used. The unidirectional CFRP embrace sheets, pultruded CFRP plates, and epoxy bonding and structural adhesives were provided by Weber and Broutin (UK) Ltd. The epoxy bonding and structural adhesives were used to bond the CFRP embrace sheets and pultruded CFRP plates, respectively in according with the manufacturer's recommendations. Details of the mechanical properties of these strengthening materials, taken from the manufacturer's data sheets, are summarised in Table 3.

4. Test results

Each test beam, which comprised two equal spans of 3830 mm, was loaded as shown in Fig. 1. Only test results at failure are presented here and full test results are

Table 2
Properties of internal steel reinforcing bars

Bar diameter (mm)	Yield strength, f_y (N/mm^2)	Ultimate strength, f_u (N/mm^2)	Young's modulus, E_s (kN/mm^2)
6 (plain round mild steel stirrups)	308	355	200
8 (high yield deformed steel bars)	505	605	200
16 (high yield deformed steel bars)	520	630	201
20 (high yield deformed steel bars)	510	615	200

Table 3
Properties of strengthening materials

Material property	Bonding adhesive	Structural adhesive	CFRP sheet	CFRP plate
Compressive strength (N/mm^2)	80	85	N/A	N/A
Tensile strength (N/mm^2)	17	19	3900	2500
Young's modulus (kN/mm^2)	5.0	9.8	240	150
Flexural strength (N/mm^2)	28	35	N/A	N/A
Bond to concrete (N/mm^2)	4.0	20.0	N/A	N/A

Table 4
Experimental results at failure of test specimens

Beam no.	Failure modes	P_u (kN)	ξ
H1	1	138.0	1.00
H2	2 followed by 1	152.3 (121.5[a])	1.10 (0.88[a])
H3	3	172.9	1.25
H4	3	162.6	1.18
H5	3	162.6	1.18
H6	2 followed by 3	172.9 (121.5[a])	1.25 (0.88[a])
S1	1	83.6	1.00
S2	4	121.8	1.46
S3	3	121.8	1.46
S4	3	170.5	2.04
S5	4	111.7	1.34
E1	1	149.7	1.00
E2	3	178.6	1.19
E3	3	207.0	1.38
E4	3	231.4	1.55
E5	3	174.6	1.17

P_u = total ultimate load (=2P where P is the mid-span point load); ξ = ultimate load enhancement ratios.
[a] Tensile rupture of the CFRP sheets occurred over the central support.

given elsewhere [12–14]. Failure modes of test specimens are summarised in Table 4 and described below.

4.1. Failure Mode 1

Conventional ductile flexural failure due to yielding of the internal tensile steel reinforcement followed by concrete crushing at both the central support and mid-span sections occurred for the three control beams H1, S1 and E1 as shown in Fig. 2 for beam E1.

4.2. Failure Mode 2

Beams H2 (see Fig. 3) and H6 exhibited tensile rupture of the CFRP sheets over the central support at 80% and 70% of each beam failure load, respectively. Tensile rupture of CFRP laminates did not cause complete collapse of beams H2 and H6. As the load increased beyond tensile rupture of the CFRP sheets, beam H2 failed in a conventional ductile flexural failure similar to that of the control beam H1 and peeling failure of the concrete cover attached to the soffit sheets in beam H6 occurred. Rupture of the CFRP sheets was sudden and accompanied by a loud noise indicating a rapid release of energy.

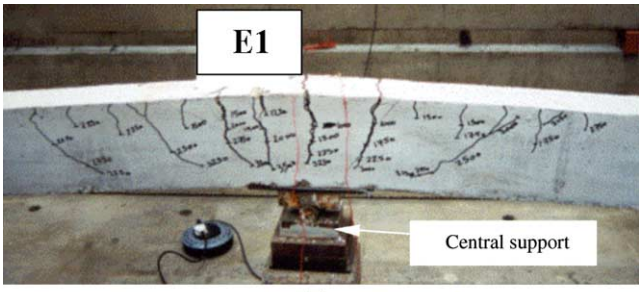

(a)

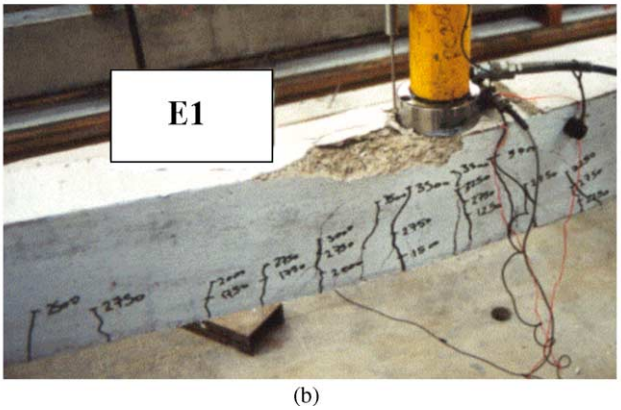

(b)

Fig. 2. Conventional ductile failure of control beam E1. (a) Over central support; (b) at mid-span.

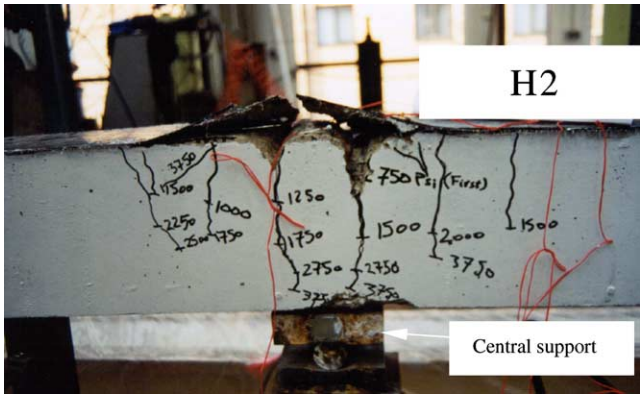

Fig. 3. Tensile rupture of the CFRP sheets (beam H2).

4.3. Failure Mode 3

Peeling failure of the concrete cover along the steel reinforcement level adjacent to the external CFRP laminates (see Fig. 4 for beam H5) occurred for a large number of strengthened beams in the test programme as given in Table 4. It was brittle, explosive and was followed immediately by beam failure. Extending the CFRP sheet to cover the entire negative moment zone such as in beams H3, E2, E4 and E5 or the entire positive moment zone such as in beams S4 and E3 did not prevent peeling failure of the cover concrete. However, beams E5 and E2 strengthened with different form of CFRP laminates, they exhibited similar peeling failure of the concrete cover adjacent to the CFRP laminates.

4.4. Failure Mode 4

CFRP sheet separation without concrete attached was noticed in beams S2 (Fig. 5) and S5. It was accompanied by a little noise before beam failure indicating impending failure of the adhesive. This may be as a result of the low compressive strength of concrete, especially in case of beam S5, which affects the bond strength at the adhesive/concrete interface.

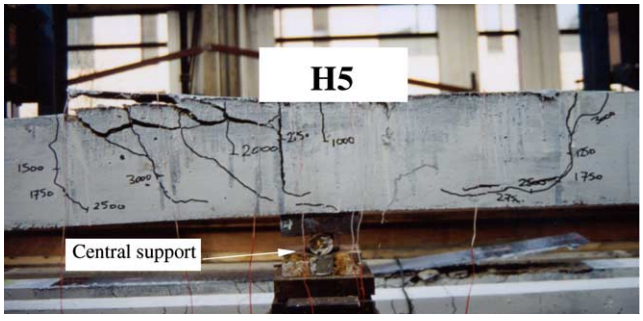

Fig. 4. Peeling failure of the cover concrete (beam H5).

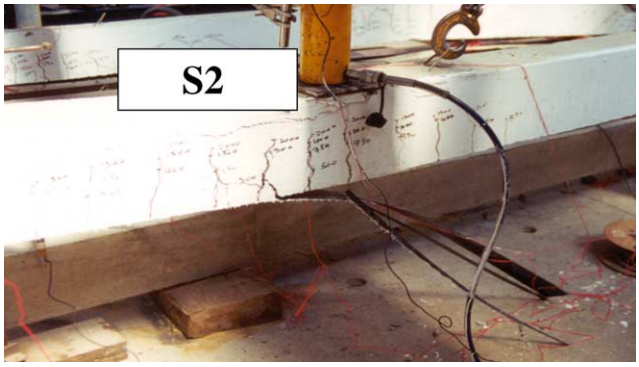

Fig. 5. CFRP sheet separation without concrete cover (beam S2).

5. Enhancement of load and moment capacities

The failure loads and ultimate load enhancement ratios, ξ (the ratio between the ultimate load of a strengthened beam and that of the corresponding unstrengthened control beam) for all tested beams are summarised in Table 4. It should be noted that the concrete compressive strengths of the control beams (24–26 MPa) are much lower than those of strengthened beams (33–47.8 MPa) as given in Table 1. Therefore, the enhancement ratios of the strengthened beams are likely to be higher than would be the case if the same compressive strength of concrete was used for control and strengthened beams in each group. The quality of the concrete also influences the performance of strengthened beams, especially with regard to the bond strength at the adhesive/concrete interface. This can be confirmed by comparing the notable difference of the failure loads of test specimens S4 and S5 (with concrete compressive strength of 42.8 and 24.4 MPa, respectively).

For a specified length of CFRP sheets, there was an optimum number of CFRP layers above which the beam load capacity was not improved (beams H3 and H4 in group H and beams S2 and S3 in group S), as indicated in Table 4. Increasing the length of the CFRP sheets was found to increase the load capacity of the strengthened beams as in the case of beams H3 and H5 in group H and beams S3 and S4 in group S. However, when tensile rupture is likely to occur, increasing the CFRP sheet length was not effective. This can be noticed by comparing the load at which tensile rupture of the CFRP sheets occurred over the central support for beams H2 and H6 (121.5 kN for both beams as indicated in Table 4). After tensile rupture, beam H2 behaved as an unstrengthened beam similar to the control beam H1. However the failure load of beam H2 (152.3 kN) is higher than that of the control beam H1 (138.0 kN) due to the difference in the concrete compressive strength. Using CFRP sheets of equivalent total tensile load capacity to the CFRP plates produced nearly the same load capacity (beams E2 and E5). Strengthening the top surface at the central support and the beam soffit was found to be the most effective arrangement of the CFRP laminates to enhance the beam load capacity such as in beams H6 and E4.

The failure moments and the ultimate moment enhancement ratios, η (the ratio between the ultimate moment of a strengthened section in a strengthened beam and that of the corresponding section in the respective unstrengthened control beam) for all tested beams are presented in Table 5. The negative and positive bending moments given in Table 5 were calculated on the basis of satisfying equilibrium using the measured end support reaction and mid-span applied load, $P(=P_u/2)$. Table 5 indicates that increasing the number of CFRP layers increased the moment enhancement ratio of a strengthened section up to a certain amount above which no further enhancement in the moment capacity could be achieved. For example, beams H2, H3 and H4 exhibited an increase in the negative moment capacity of the strengthened section at the central support due to increasing the number of CFRP layers, whereas increasing the number of CFRP layers between beams S4 and S5 decreased the positive moment capacity.

Tables 4 and 5 show that using CFRP laminates for the strengthening of continuous beams is an effective technique; the load and moment capacities can be increased by factors of up to 2.04 and 3.34, respectively, as was the case for beam S4. By comparing the ultimate load enhancement ratio of a strengthened beam and the moment enhancement ratio of a strengthened section in the same beam, it can be concluded that the latter was significantly higher than the former. Such a conclusion is not valid for simply supported beams strengthened with external reinforcement where the moment and load enhancement ratios are always the same.

6. Beam ductility

The deflection ductility index, μ_Δ, used for simply supported beams by Mukhopadhyaya et al. [15] is adopted to measure the ductility of the continuous beams tested by the authors as given in Table 5. The deflection ductility index, μ_Δ, is defined as:

$$\mu_\Delta = \frac{\Delta_u}{\Delta_y} \tag{1}$$

where Δ_u is the mid-span deflection at beam ultimate load and Δ_y is the mid-span deflection at the lower yielding load of the tensile reinforcement over the central support or the beam mid-span. As can be seen from Table 5, all strengthened beams exhibited less ductility than the corresponding unstrengthened control beams. Only beam H2 showed nearly similar ductility at failure as that of the control beam H1 because both beams

Table 5
The moment, moment enhancement ratio, η and ductility index at failure of test specimens

Beam no.	M_h (kN m)	M_s (kN m)	η	μ_Δ
H1	21.21	56.78	1.00	4.10
H2	31.60	61.00	1.49 (h)	4.34 (1.83[a])
H3	46.48	59.56	2.19 (h)	1.35
H4	53.07	51.32	2.50 (h)	1.74
H5	35.00	64.27	1.65 (h)	2.64
H6	28.26[a]	70.24	1.33 (h); 1.24 (s)	3.46 (1.71[a])
S1	57.77	11.13	1.00	12.85
S2	71.28	22.67	2.04 (s)	6.21
S3	66.90	24.72	2.22 (s)	2.93
S4	88.97	37.15	3.34 (s)	2.52
S5	50.18	28.36	2.55 (s)	1.00[b]
E1	54.49	44.41	1.00	6.12
E2	79.78	45.64	1.46 (h)	3.58
E3	53.56	72.35	1.63 (h)	3.21
E4	77.00	72.29	1.41 (h); 1.63 (s)	2.10
E5	77.42	44.87	1.42 (h)	2.60

M_h and M_s = ultimate negative and positive bending moments; η = ultimate moment enhancement ratio; (h) = over the central support section and (s) = at mid-span section.
[a] Tensile rupture of the CFRP sheets occurred over the central support.
[b] There was no ductility.

failed in flexure at the ultimate load level. However, if the ductility was considered at tensile rupture of the CFRP sheets, beam H2 would have less ductility than that of the control beam H1. Increasing the thickness and length of CFRP laminates was found to decrease the beam ductility.

7. Predictions of capacity of tested beams

Simplified methods for estimating the flexural load capacity and the elastic shear stresses at the adhesive/concrete interface at failure of beams tested are given in this section.

7.1. Flexural capacity of beams tested

The prediction of the flexural capacity of the test specimens was based on satisfying equilibrium conditions and assuming that both the mid-span and central support sections have high ductility and reached their flexural capacities M_{us} and M_{uh}, respectively as shown in Fig. 6(a). Accordingly, from equilibrium considerations, the applied point load, P_t, at the beam mid-span is calculated from (beam self weight is neglected):

$$P_t = \frac{2}{L}(M_{uh} + 2M_{us}) \tag{2}$$

When Eq. (2) is applied to beams H4, H5, S2 and S3, it was found that the bending moment at the unstrengthened section next to the sheet end (the end closer to the end support for soffit sheets) is higher than the moment capacity of that section. In such cases, the mid-span point load, P_t, for beams H4 and H5 was calculated from (see Fig. 6(b)):

$$P_t = \frac{2}{L}\left(\frac{M_{us}L_1 + M_{he}L}{L - L_1} + 2M_{us}\right) \tag{3}$$

and that for beams S2 and S3 was determined from (see Fig. 6(c)):

$$P_t = \frac{2}{L}\left(M_{uh} + \frac{2L}{L - L_2}M_{se}\right) \tag{4}$$

where M_{he} and M_{se} are the negative and positive moment capacities of the unstrengthened sections at the CFRP sheet end, respectively, and L_1 and L_2 are the lengths of the CFRP sheets over the central support and at the beam soffit, respectively as shown in Fig. 6(b) and (c). The calculation of flexural capacities of different critical sections as required by Eqs. (2)–(4) is based on the numerical method presented in Appendix A.

The flexural mechanism of failure presented above is only suitable for test specimens in which ductile behaviour was dominant, such as the control beams H1, S1 and E1. It may also be used for test specimens partly strengthened over the central support or at soffit mid-spans where ductile failure occurred at the unstrengthened section and then brittle flexural failure took place at the strengthened section due to either concrete crushing or CFRP laminate rupture. However, the authors applied the flexural mechanism to the beams with CFRP laminates bonded over the central support or at mid-span soffit to calculate the reserve capacity of test specimens if brittle peeling or separation failure of CFRP laminates was prevented. For beams fully strengthened with CFRP bonded over the central support and at the mid-span soffit where beam failure was

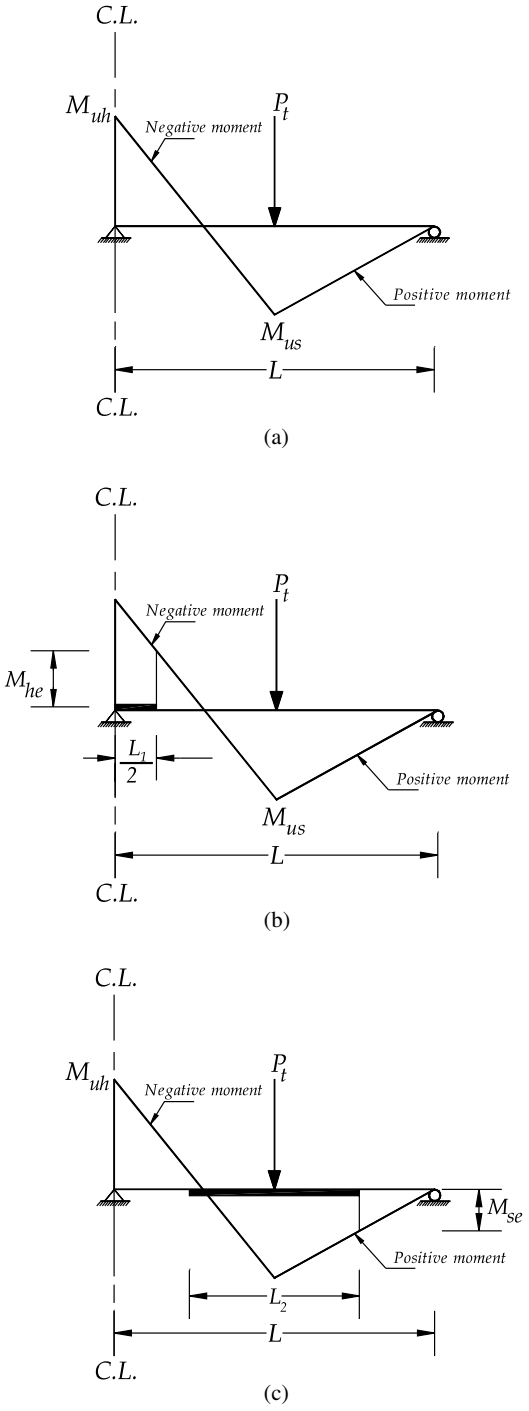

Fig. 6. Ultimate positive and negative moments at critical sections of continuous beams tested. Critical sections over the central support and at mid-span (a), at the plate end and mid-span (b), over the central support and the plate end (c).

brittle and sudden, the flexural mechanism is not applicable. Table 6 presents the total load capacity, $P_{th}(=2P_t)$, obtained from Eqs. (2)–(4) for all test specimens except H6 and E4 and the ratio, $\lambda_1(=P_u/P_{th})$, between experimental and theoretical load capacities. The calculated negative and positive flexural capacities of different critical sections using Eq. (A.8) are also given in Table 6. Good agreement between flexural load capacity obtained from current theoretical method and that measured during experiments for beams failed in flexural mode such as the three control beams (H1, S1 and E1) and beam H2 failed due to tensile rupture of the CFRP laminates. This comparison also shows that, apart from beams H4, S4 and S5, the strengthened beams tested were close to developing their full flexural capacity.

7.2. Interface shear stresses of beams tested

Several analytical methods have been developed for predicting peeling failure of RC beams strengthened with external plates [16,17]. These methods, however, were found to be derived for simply supported RC beams strengthened with external reinforcement and, therefore, are not directly applicable to continuous RC beams. As elastic theory has been widely used by a large number of researchers [1,11,18–20], it is applied to the beams tested in order to estimate interface shear stresses between the adhesive and concrete at failure.

According to the elastic theory, the longitudinal shear stress at the adhesive level, τ, is calculated from Eq. (5) below:

$$\tau = \frac{V n_f t_f y_f}{I_c} \tag{5}$$

where V is the shear force calculated at beam failure; n_f is the CFRP laminate modular ratio ($=E_f/E_c$ where E_f and E_c are the elastic moduli of the CFRP laminate and concrete, respectively); t_f is the thickness of the CFRP laminate; y_f is the depth of the CFRP laminate measured from the neutral axis to the centroid of the CFRP laminate and I_c is the transformed second moment of area of the cracked reinforced concrete cross-section with external CFRP laminates in terms of concrete.

Table 6 presents the peak shear stresses, τ, along the CFRP laminate length calculated at the experimental failure load of the CFRP laminates i.e. at rupture, separation or peeling of the concrete cover attached to the CFRP laminates. The peak shear stresses along the adhesive level ranged from 0.80 to 1.55 N/mm^2 for beams failed due to peeling failure apart from the soffit CFRP sheets in beam H6. Conversely, the peak shear stresses calculated according to the elastic theory for beams that exhibited tensile rupture of the CFRP sheets such as H2 and H6 (top sheets) were less than 0.80 N/mm^2. This listed data conformed to the 0.80 N/mm^2 upper limit for interface shear stresses proposed in the Concrete Society Technical Report 55 [11]. In other words, when the elastic shear stresses along the adhesive level are found to exceed 0.80 N/mm^2, peeling failure would be expected to occur.

Table 6
Theoretical negative and positive flexural moment capacities, load capacity and elastic shear stresses at concrete/adhesive interface of test specimens

Beam no.	M_{uh} (kN m)	M_{us} (kN m)	P_{th} (kN)	λ_l	τ (MPa)
H1	12.52[a]	50.58	118.73	1.16	N/A
H2	33.83	60.33	161.35	0.94	0.48
H3	69.96	57.83	193.86	0.89	1.32
H4	87.08 (11.20[b])	57.83	210.19	0.77	1.55
H5	75.30 (11.67[b])	60.51	165.22	0.98	1.05
H6	33.96	70.24	–[c]	–[c]	0.47[d]/0.16[e]
S1	49.78	10.68	74.30	1.13	N/A
S2	60.23	33.81 (11.61[f])	113.66	1.07	0.81
S3	57.98	70.21 (11.22[f])	109.60	1.11	1.12
S4	60.23	74.63	218.77	0.78	1.54
S5	54.25	81.06	225.97	0.49	1.15
E1	41.20	41.20	129.09	1.16	N/A
E2	82.97	42.44	175.30	1.02	0.80
E3	42.64	85.24	222.58	0.93	0.82
E4	84.17	84.17	–[c]	–[c]	0.97[d]/0.75[e]
E5	83.35	42.48	175.78	0.99	0.79

[a] Moment capacity calculated based on ultimate strength of steel bars as this beam exhibited very high rotational capacity before failure.
[b] Moment capacity of negative unstrengthened section at the central support laminate end.
[c] Beam is fully strengthened over the central support and mid-span soffit, therefore flexural mechanism is not applicable.
[d] Interface shear stresses calculated at the top CFRP laminates.
[e] Interface shear stresses calculated at the soffit CFRP laminates.
[f] Moment capacity of positive unstrengthened section at the soffit laminate end.

8. Conclusions

Test results at failure of 16 RC beams with external CFRP laminates have been presented. A simple method to predict the flexural load capacity of beams tested has been developed. The flexural failure of continuous beams is assumed when two critical sections attained their flexural capacities that are estimated based on satisfying the compatibility and equilibrium conditions. The elastic shear stresses at the adhesive/concrete interface is calculated at beam failure and compared with the limiting value suggested by the Concrete Society Technical Report 55 [11]. Based on the work described in this paper, the following conclusions are drawn:

1. All strengthened beams exhibited a higher beam load capacity but lower ductility compared with their respective unstrengthened control beams.
2. Brittle peeling failure of the concrete cover adjacent to the CFRP sheets was the dominant failure mode of the strengthened beams tested. However, most beams were close to achieving their flexural capacity.
3. Increasing the CFRP sheet length to cover the entire negative or positive moment zones did not prevent peeling failure of the CFRP laminate and was found to be ineffective when tensile rupture of the CFRP sheets was the failure mode.
4. Unlike simply supported beams, the enhancement of the bending moment capacity of a continuous beam due to external strengthening was found to be higher than that of the load capacity of the continuous beam.
5. The shear stresses calculated along the adhesive level using elastic theory should not exceed 0.80 N/mm^2 to avoid brittle peeling failure of FRP laminates.

Acknowledgements

The second author acknowledges the grant provided from the Egyptian government to fulfil this research. The experimental work described in this paper was conducted in the Heavy Structures Laboratory in the University of Bradford; the assistance of the laboratory staff is acknowledged. The authors are grateful to Weber and Broutin (UK) Ltd. for providing the CFRP reinforcement and the associated priming and bonding materials for the research.

Appendix A. Bending capacity of strengthened sections

In this appendix, the flexural capacity of critical sections as required by Eqs. (2)–(4) is based on the numerical method presented below [21,22]. The following assumptions are considered:

1. Plane sections before bending remain plane after bending.
2. The stress–strain relationships of concrete in compression and steel reinforcement in both tension and compression proposed by BS8110 [23] is adopted.
3. A linear stress–strain relationship of the CFRP laminate up to rupture is assumed.

4. The tensile strength of concrete is ignored.
5. Perfect bond exists between CFRP laminates and concrete surface.

A.1. Size of CFRP laminates at concrete crushing and CFRP rupture

At the instant of failure, either the concrete strain ε_c at the extreme compression fibre or the CFRP laminates strain ε_f at the extreme tension fibre reaches the respective ultimate strain, that is $\varepsilon_c = \varepsilon_{cu} = 0.0035$ (concrete crushing) or $\varepsilon_f = \varepsilon_{fu}$ (tensile CFRP rupture), where ε_{cu} and ε_{fu} are the ultimate strains of concrete and CFRP laminates, respectively. The area of the CFRP laminates that distinguishes between concrete crushing and tensile rupture of the CFRP laminates is first estimated as follows.

- Calculate the neutral axis depth, x, the tensile steel bar strain, ε_s, and the compressive steel bar strain, ε'_s, from the strain profile shown in Fig. 7(b) where $\varepsilon_c = \varepsilon_{cu} = 0.0035$ and $\varepsilon_f = \varepsilon_{fu}$ as given below:

$$x = \frac{0.0035}{0.0035 + \varepsilon_{fu}} d_f \tag{A.1}$$

$$\varepsilon'_s = 0.0035 \frac{x - d'}{x} \tag{A.2}$$

$$\varepsilon_s = 0.0035 \frac{d - x}{x} \tag{A.3}$$

  where d_f, d' and d are the depths of CFRP laminates, compression steel bars and tension steel bars from the top face of the section as shown in Fig. 7(a).
- Consequently, stresses in the tensile steel bars, f_s, and compressive steel bars, f'_s, are determined from the bilinear stress–strain relationship for the steel reinforcement [23].
- The concrete compressive force C is calculated from:

$$C = k_1 k_2 f_{cu} b x \tag{A.4}$$

  where k_1 and k_2 are two parameters, defining the idealised rectangular stress block of concrete in compression as shown in Fig. 7(c), b is the section width and f_{cu} is the concrete cube strength. k_1 is the ratio of the average compressive stress to the concrete cube strength f_{cu} and k_2 is the ratio of the depth of the idealised rectangular stress block to the neutral axis depth. They can be calculated according to the assumed strain ε_c at the extreme compression fibre [21,23]; $k_1 = 0.67$ and $k_2 = 0.9$ for $\varepsilon_c = \varepsilon_{cu} = 0.0035$.
- Considering equilibrium of the internal forces, the area A_{fl} of CFRP, where both concrete crushing and tensile rupture of CFRP laminates simultaneously occur, is calculated from:

$$A_{fl} = \frac{0.603 f_{cu} b x + A'_s f'_s - A_s f_s}{f_{fu}} \tag{A.5}$$

  where f_{fu} is the ultimate tensile strength of CFRP laminates, and A_s and A'_s are the internal longitudinal tension and compression steel reinforcement areas, respectively.

A.2. Estimation of bending capacity

By comparing the actual CFRP area A_f used with A_{fl} obtained from Eq. (A.5), strains in either the concrete extreme compression fibre or CFRP laminates may be predicted; that is:

$$\begin{aligned} &\varepsilon_f = \varepsilon_{fu} \quad A_f \leqslant A_{fl} \\ &\varepsilon_c = \varepsilon_{cu} \quad A_f > A_{fl} \end{aligned} \tag{A.6}$$

For complete determination of the strain distribution, the neutral axis depth, x, is initially assumed and the correct value is iteratively determined when the equilibrium of internal forces is satisfied. Strains and stresses in different materials can then be calculated. The summation of the internal forces, Q, can be determined:

$$\begin{aligned} Q &= C + C_s - T_s - T_f \\ &= k_1 k_2 f_{cu} b x + A'_s f'_s - A_s f_s - A_f f_f \end{aligned} \tag{A.7}$$

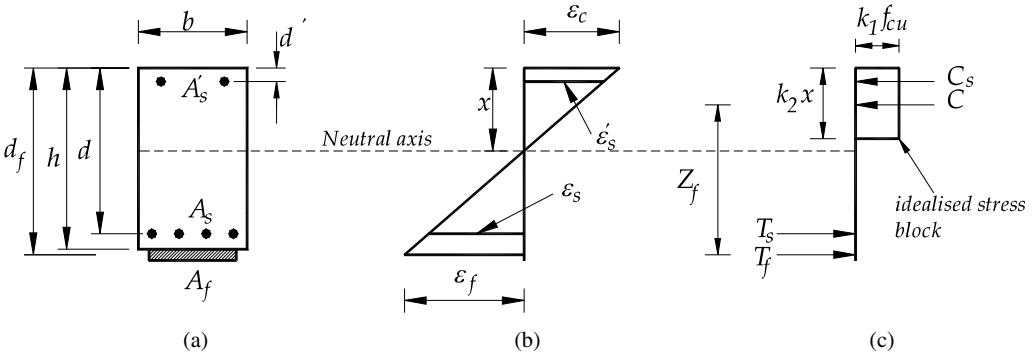

Fig. 7. Strains, stresses and forces on RC section with externally bonded CFRP laminates at failure. (a) RC section with FRP; (b) section distribution; (c) stresses and forces.

where $C_s = A'_s f'_s$ = compressive force in steel reinforcement above the neutral axis, $T_s = A_s f_s$ = tensile force in steel reinforcement below the neutral axis and $T_f = A_f f_f$ = tensile force in external CFRP laminates as shown in Fig. 7. The equilibrium of the internal forces is satisfied when the summation of forces, Q, is zero or lies within an accepted tolerance (say $|\frac{Q}{C+A'_s f'_s}| < 10^{-6}$). If not, the neutral axis depth, x, is iteratively adjusted until equilibrium of forces is satisfied. Consequently, the flexural strength, M_u, is calculated by taking moments of internal forces about the level of tensile steel as follows:

$$M_u = k_1 k_2 f_{cu} b x \left(d - \frac{k_2 x}{2}\right) + A'_s f'_s (d - d') + A_f f_f (d_f - d) \quad \text{(A.8)}$$

References

[1] Jones R, Swamy RN, Charif A. Plate separation and anchorage of reinforced concrete beams strengthened by epoxy-bonded steel plates. Struct Eng, Inst Struct Engrs, London 1988;66(5/1):85–94.

[2] Swamy RN, Mukhopadhyaya P. Debonding of carbon-fibre-reinforced polymer plate from concrete beams. Proc Inst Civil Engrs Struct Buildings 1999;134:301–17.

[3] Garden HN, Hollaway LC. An experimental study of the influence of plate end anchorage of carbon fibre composite plates used to strengthen reinforced concrete beams. Compos Struct 1998;42:175–88.

[4] Arduini M, Nann A, Tommaso AD, Focacci F. Shear response of continuous RC beams strengthened with carbon FRP sheets. Non-metallic (FRP) reinforcement for concrete structures. In: Proceedings of the Third International Symposium (FRPRCS-3), Sapporo, Japan, October, vol. 1, 1997. p. 459–66.

[5] Spadea G, Bencardino F, Swamy RN. Structural behaviour of composite RC beams with externally bonded CFRP. J Compos Construct, ASCE 1998:132–7.

[6] Lamanna AJ, Bank LC, Scott DW. Flexural strengthening of reinforced concrete beams using fasteners and fiber-reinforced polymer strips. ACI Struct J 2001;98(3):368–76.

[7] Khalifa A, Tumialan G, Nanni A, Belarbi A. Shear strengthening of continuous reinforced beams using externally bonded carbon fiber reinforced polymer sheets. In: Fourth International Symposium on Fiber Reinforced Polymer Reinforcement for Reinforced Concrete Structures. American Concrete Institute; 1999. p. 995–1008.

[8] Grace NF, Soliman AK, Abdel-Sayed G, Saleh KR. Strengthening of continuous beams using fiber reinforced polymer laminates. In: Fourth International Symposium on Fiber Reinforced Polymer Reinforcement for Reinforced Concrete Structures. American Concrete Institute; 1999. p. 647–57.

[9] Tann DB, Delpak R. Shear strengthening of continuous reinforced concrete beams using externally bonded carbon fibre sheets. Concrete Communication Conference 2000, The 10th BCA Annual Conference on Higher Education and the Concrete Industry, 29–30 June, Birmingham, UK, 2000. p. 325–38.

[10] ACI Committee 440. Starte-of-the-art report on fiber reinforced plastic reinforcement for concrete structures, Report ACI 440R-96. Detroit, USA: American Concrete Institute; 1996.

[11] Concrete Society. Design guidance for strengthening concrete structures using fibre composite materials. Concrete Society Technical Report No. 55, 2000. 71p.

[12] El-Refaie SA, Ashour AF, Garrity SW. Tests of reinforced concrete continuous beams strengthened with carbon fibre sheets. The 10th BCA Annual Conference on Higher Education and the Concrete Industry, 29–30 June, Birmingham, UK, 2000. p. 187–98.

[13] El-Refaie SA, Ashour AF, Garrity SW. Strengthening of reinforced concrete continuous beams with CFRP composites. The International Conference on Structural Engineering, Mechanics and Computation, Cape Town, South Africa, 2–4 April, 2001. p. 1591–8.

[14] El-Refaie SA, Ashour AF, Garrity SW. Sagging strengthening of continuous reinforced concrete beams using carbon fibre sheets. The 11th BCA Annual Conference on Higher Education and the Concrete Industry, Manchester, UK, 3–4 July, 2001. p. 281–92.

[15] Mukhopadhyaya P, Swamy RN, Lynsdale C. Optimizing structural response of beams strengthened with GFRP plates. J Compos Construct, ASCE 1998:87–95.

[16] Smith ST, Teng JG. FRP-strengthened RC beams. I: Review of debonding strength models. Eng Struct 2002;24(4):385–95.

[17] Smith ST, Teng JG. FRP-strengthened RC beams. II: Assessment of debonding strength models. Eng Struct 2002;24(4):397–417.

[18] Mukhopadhyaya P, Swamy N. Interface shear stress: A new design criterion for plate debonding. J Compos Construct 2001;5(1):35–43.

[19] El-Mihilmy MT, Tedesco JW. Prediction of anchorage failure for reinforced concrete beams strengthened with fiber-reinforced polymer plates. ACI Struct J 2001:301–14.

[20] Roberts TM. Approximate analysis of shear and normal stress concentrations in the adhesive layer of plated RC beams. Struct Eng, Inst Struct Engrs, London 1989;67(12/20):229–33.

[21] Ashour AF. Size of FRP laminates to strengthen reinforced concrete sections in flexure. Struct Buildings J, Inst Civil Engrs 2002;152(3):209–17.

[22] El-Mihilmy MT, Tedesco JW. Analysis of reinforced concrete beams strengthened with FRP laminates. J Struct Eng, ASCE 2000;126(6):684–91.

[23] British Standards Institution. Structural use of concrete: code of practice for design and construction. BS8110, Part 1, Milton Keynes, UK, 1997.